BMC Cancer

RESEARCH

Open Access

Identification of alternative lengthening of telomeres-related genes prognosis model in hepatocellular carcinoma

FanLin Zeng[1†], YuLiang Chen[2] and Jie Lin[3*]

Abstract

Background Hepatocellular carcinoma (HCC) is a common malignant tumor worldwide, characterized by high mortality. This study aimed to explore the prognostic value and function of alternative lengthening of telomeres (ALT)-related genes in HCC.

Methods Differentially expressed genes (DEGs) were identified based on The Cancer Genome Atlas (TCGA) and then intersected with ALT-related genes to obtain ALTDEGs. Risk score model was constructed using the least absolute shrinkage and selection operator (LASSO) algorithm and Cox regression and validated with Gene Expression Omnibus (GEO) datasets. The predictive efficacy of the risk score and ALTs-score was evaluated by Kaplan-Meier curves, time-ROC curves, and the nomogram analyses. The impacts of SMG5 silencing on the HCC cell behaviors were assessed by CCK-8, wound healing, and Transwell assays.

Results A total of 500 ALTDEGs were screened and 13 genes (CDCA8, SMG5, RAD54B, FOXD2, NOL10, RRP12, CCT5, CCT4, HDAC1, DDX1, HRG, HDAC2, and PPP1CB) were identified for constructing a prognostic model. The overall survival (OS) curves, time-ROC curves, and nomograms based on the risk score or ALTs-score were developed to optimally predict the survival of HCC patients. ALTs-score was correlated with immune infiltration and confirmed its value in predicting immunotherapy outcomes. Furthermore, RT-qPCR demonstrated that eight risk signature genes were up-regulated in HCC cells. SMG5 silencing suppressed the proliferation, migration, and invasion of HCC cells. It was also found that SMG5 silencing reduced C-circle level in SNU-387 cells.

Conclusion We identified new ALT-related prognostic biomarkers for HCC. SMG5 knockdown inhibited the HCC progression, which might be a promising target for HCC therapy.

Highlights

- 13 ALTDEGs were identified for constructing a risk model model.
- Risk model and ALTs-score model could be used for HCC prognosis.
- 13 ALTDEGs could serve as prognostic and diagnostic biomarkers for HCC.
- SMG5 knockdown suppressed the proliferation, migration, and invasion of HCC cells.

†FanLin Zeng is the first author.

*Correspondence:
Jie Lin
linjie7523@163.com

Full list of author information is available at the end of the article

Keywords Hepatocellular carcinoma, Alternative lengthening of telomeres, Prognostic model

Introduction

Primary liver cancer accounted for over 906,000 new cases and 830,000 deaths globally in 2020, according to GLOBOCAN statistical data, making it the sixth most prevalent cancer to be diagnosed and the third largest cause of cancer-related deaths. Hepatocellular carcinoma (HCC) constitutes 75-85% of all primary liver cancer cases [1]. Virus infection, contamination with aflatoxins, excessive alcohol intake, and smoking are predisposing factors for HCC. Currently, the primary options for the HCC treatment include hepatic resection, liver transplantation, radiation therapy, local ablation, transarterial therapy, and systemic therapy [2]. However, as HCC lacks symptoms in its early phases, the majority of patients are typically diagnosed at an advanced stage, missing the chance for these treatments [3]. Consequently, it is important to further explore the molecular mechanisms of HCC and search for effective biomarkers and potential therapeutic targets.

Telomeres are located at the ends of chromosomes and are safeguarded by a series of telomere-binding proteins, ensuring they are not perceived as DNA double-strand breaks [4]. As somatic cells divide, their telomeres shorten, causing a buildup of DNA damage that initiates cellular senescence [5]. The maintenance of telomere length is essential for the proliferation of malignant cells. Telomerase sustains telomere length primarily through the addition of the TTAGGG repeat sequence to chromosome ends or the alternative lengthening of telomeres (ALT) mechanism, which largely depends on homologous recombination (HR) between sister chromatids [6]. Telomere shortening without telomerase causes ssDNA accumulation at the telomere region, and the HR counters the ssDNA and elongates the telomere via the DNA damage response pathway [7]. Clustering of telomeres can occur at the G1 and S phases of the cell cycle, with three types of telomeric HR being distinguished by the mode of telomeric DNA exchange: equivalent telomeric sister chromatin exchange, inequivalent T-SCE, and non-sister chromatid exchange [8]. ALT occurs in 5-10% of all cancers, with a significantly higher prevalence in pancreatic neuroendocrine tumors, complex karyotype sarcomas, isocitrate dehydrogenase-mutant astrocytomas, neuroblastoma, and chromophobe HCC [9]. In HCC, the incidence of ALT is between 6% and 10% [10]. ALT has been recognized as an effective diagnostic and prognostic biomarker for specific cancer types. It is reported that patients with soft tissue sarcomas characterized by an ALT phenotype generally experience poorer prognoses than those with ALT-negative tumors [11]. A bioinformatics study demonstrated that the ALT-associated 22-gene risk score is a strong prognostic indicator in lower-grade glioma patients [12]. Furthermore, NFRKB, a telomere-associated protein, is highly expressed in HCC and correlates with reduced overall survival (OS) times and a worse prognosis [13]. However, the prognostic relevance of ALT-related genes in HCC and their impact on biological processes are not fully understood.

In this investigation, we identified new ALTDEGs-related biomarkers and developed a risk model and an ALTs-score model to predict the prognosis of HCC. Moreover, targeting SMG5 effectively diminished HCC cell proliferation, migration, invasion, and C-circle level, suggesting SMG5 might be a potential target for HCC treatment.

Materials and methods

Data collection

Supplementary Fig. 1 illustrates the process of this study. Firstly, using the TCGAbiolinks package in the R software (version 4.1.2), the liver hepatocellular carcinoma (LIHC) dataset from The Cancer Genome Atlas (TCGA) (https://portal.gdc.cancer.gov/) was obtained. This data set comprised 374 LIHC samples and 50 paraneoplastic samples. In the UCSC Xena database (http://genome.ucsc.edu), corresponding clinical data were downloaded (Supplementary Table 1). The count sequencing data were normalized utilizing the limma package. GSE25097 (GPL6947 platform), GSE46408 (GPL4133 platform), and GSE84402 (GPL570 platform) were acquired from the Gene Expression Omnibus (GEO, http://www.ncbi.nlm.nih.gov/geo/) via the GEOquery package. GSE25097 comprises 268 HCC samples and 243 paraneoplastic normal samples. GSE46408 includes six HCC samples and six paraneoplastic normal samples. GSE84402 contains 14 HCC samples and 14 paraneoplastic normal samples. A total of three GEO datasets were used as validation sets.

We entered the keyword "Alternative Lengthening of Telomeres" and selected the "Protein Coding" option in the GeneCards database (https://www.genecards.org/), resulting in 309 ALT-related genes (ALTRGs). Additionally, a total of 411 ALTRGs were obtained from PubMed website (https://pubmed.ncbi.nlm.nih.gov/). A total of 625 ALTRGs were identified between two databases. The somatic mutation data of the TCGA-LIHC dataset, including single nucleotide polymorphism (SNP) data, were loaded from the TCGA database and visualized using the maftools. The copy number variation (CNV) data was download via TCGAbiolinks package, which were then analyzed by GISTIC 2.0.

Combination of validation datasets

The GSE25097, GSE46408, and GSE84402 datasets were integrated, and the batch effect was removed by the sva package in the R software. The combined datasets were then standardized using the limma package.

Identification of ALT-related differentially expressed genes (ALTRDEGs)

Differentially expressed genes (DEGs) were identified with the limma R package. To uncover as many HCC-related genes as possible, a criterion of $|\log FC| > 0$ and $p < 0.05$ was used [14, 15]. This approach ensures that small but potentially significant changes in expression are not missed, especially in complex regulatory networks or in cases where small changes in expression lead to large phenotypic effects, and p-value filters contribute to ensuring that the changes detected are statistically significant. ALTRDEGs were obtained by taking the intersection of ALTRGs and DEGs using the Venn tool (https://bioinformatics.psb.ugent.be/webtools/Venn/). The volcano plot and differential ordering plot of ALTRDEGs were generated using the ggplot2 package.

Functional enrichment analysis

Gene Ontology (GO) analysis includes three terms: biological process (BP), cellular component (CC), and molecular function (MF). GO and Kyoto Encyclopedia of Genes and Genomes (KEGG) enrichment analysis of ALTRDEGs was performed utilizing the clusterProfiler package. Statistical significance was determined when the $p < 0.05$ and FDR < 0.05.

Gene set enrichment analysis (GSEA)

The clusterProfiler R package was utilized to conduct GSEA. Gene sets were screened with a maximum size of 500 genes and a minimum size of 10 genes. Gene set c2.cp.all.v2022.1.Hs.symbols.gmt [All Canonical Pathways] (3050) was obtained through the Molecular Signatures Database (MSigDB) database (https://www.gsea-msigdb.org/gsea/msigdb) for GSEA. The screening thresholds were set at $p < 0.05$, FDR < 0.25, and $|NES| > 1$.

Gene set variation analysis (GSVA)

The "c2.cp.kegg.v7.2.symbols.gmt" file was obtained from the MSigDB database. Data adjustments were conducted via the limma package, with $p < 0.05$ marking significant differences among the subgroups.

Establishment and validation of the ALTRDEGs-based risk model and ALTs-score model

To identify prognosis-related ALTRDEGs, the least absolute shrinkage and selection operator (LASSO) analysis was executed with the glmnet package, applying a binomial family parameter and tenfold cross-validation. LASSO regression can eliminate irrelevant variables by penalizing the magnitude of the regression coefficients [16]. Using LASSO regression, we performed feature selection and developed a predictive signature. The process was run for 1000 cycles to prevent overfitting. Risk scores were calculated based on the following formula (the mRNA expression was quantified based on Fragments Per Kilobase Million):

$$\text{riskScore} = \sum_{i} \text{Coefficient}\ (\text{gene}_i) * \text{mRNA Expression}\ (\text{gene}_i)$$

In the prognostic risk model, mRNA Expression (gene_i) denotes the expression values of gene i, and Coefficient (gene_i) indicates the regression coefficient for gene i in the model. According to their median risk score, patients with HCC were allocated into low-risk and high-risk groups. ALTs scores were calculated for each sample in the TCGA-LIHC disease group using the ssGSEA algorithm with the GSVA package [17]. The ability of ALTs-score, prognosis-related ALTRDEGs, and relevant clinical parameters to predict overall survival OS in LIHC patients was evaluated employing univariate and multivariate Cox regression analyses. Time-dependent receiver operating characteristic (ROC) curve analyses were performed using the survivalROC package. The rms R package was employed to build a nomogram of the prognostic genes, ALTs-score, and clinicopathological features, with the calibration plots utilized to measure the prognostic effectiveness. On the x-axis, the nomogram-predicted survival was displayed, and the observed outcome was plotted on the y-axis, with the 45° line representing the best prediction. 1-year, 3-year, and 4-year decision curve analyses (DCA) were conducted to evaluate and compare prediction models that account for clinical outcomes, assessing the suitability of our nomogram for clinical use. The x-axis displayed the threshold probability percentage, while the y-axis showed the net benefit.

Immunotherapy and immune infiltration analysis of ALTs-score model

LIHC patients were categorized into high and low groups according to ALTs scores. Expression of ALTRDEGs in high and low groups were calculated by Mann-Whitney U test. The Immunophenoscore (IPS) was utilized to predict responses to immune checkpoint inhibitors (ICIs). Box plots of IPS for high and low groups of ALTs were generated with the ggplot package. The CIBERSORT (https://cibersort.stanford.edu/) was employed to analyze immune infiltration. The composition of 22 tumor-infiltrating immune cell types was calculated for each tumor sample, followed by a Wilcoxon test to compare immune cell infiltration differences between high and low groups.

Consensus clustering

We categorized LIHC patients into subtypes using consensus clustering with the ConsensusClusterPlus package in the R software, based on prognostic ALTRDEGs. For clustering, the number of clusters was varied from 2 to 8, with each configuration repeated 50 times, sampling 80% of the data, and using km as the algorithm and Euclidean distance. Differential expression of prognostic genes between disease subtypes were determined using the Mann-Whitney U test.

Cell culture

Human normal hepatocytes L-02 and human HCC cells SK-HEP-1 and SNU-387 were acquired from Icellbioscience Biotechnology Co., Ltd., (Shanghai, China). L-02 cells were cultured in RPMI-1640 medium with 20% fetal bovine serum (FBS; Thermo Fisher Scientific, Massachusetts, USA) and 1% antibiotics. SK-HEP-1 cells were cultivated in MEM medium supplemented by 10% FBS and 1% antibiotics. SNU-387 cells were grown in RPMI-1640 medium containing 10% FBS, 1% antibiotics, 1% GlutaMAX-1 glutamine, and 1% sodium pyruvate. All cells were grown in an incubator set to 37 °C with 5% CO_2.

Cell transfection

The siRNA targeting SMG5 (si-SMG5-1, si-SMG5-2, and si-SMG5-3; GenePharma, Shanghai, China) was used to knock down SMG5 in HCC cells. The non-targeting siRNA (si-NC) served as a negative control. Cells were seeded into 24-well plates. Upon reaching a density of about 30–50%, cells were transfected using Lipofectamine 3000 (Thermo Fisher Scientific) following the manufacturer's guidelines. Briefly, after removing the original medium, 1 mL of fresh culture medium (containing serum and no antibiotics) was added to each well. Two clean and sterile centrifuge tubes were prepared, and 25 μL of DMEM culture medium (without serum and antibiotics) was added to each tube. The siRNA (20 pmol) was added to one sterile tube, and 1 μL of Lipofectamine 3000 transfection reagent to the other. Both were gently mixed by pipetting and left at room temperature for 5 min. The culture medium containing siRNA was then gently transferred into the sterile centrifuge tube containing Lipofectamine 3000 transfection reagent. The mixture was gently inverted and mixed, followed by a 5-min incubation at room temperature. A total of 50 μL of the mixture was added dropwise to each well and gently mixed. Cells were cultured for 6 h after transfection, and the medium was changed with fresh complete culture medium. The siRNA sequences used in this study were shown in Supplementary Table 2.

Reverse transcription quantitative PCR (RT-qPCR)

Total RNA extraction from cells was performed 48 h post-transfection with Trizol reagent (Thermo Fisher Scientific). Phase separation of cell lysates in Tirol was performed by adding 120 μL of chloroform, and then 300 μL of isopropanol was added to precipitate the RNA. Then, cDNA synthesis was performed using a SweScript All-in-One First-Stand cDNA Synthesis Supermix kit (Servicebio, Wuhan, China). The qPCR was carried out on a 7500 real-time PCR system (Thermo Fisher Scientific). Target gene expression levels were determined via the $2^{-\Delta\Delta Ct}$ method. Primer sequences are provided in Supplementary Table 3.

Cell counting kit-8 (CCK8)

The 1×10^4 cells was configured in a 96-well plate. Subsequently, 90 μL of complete and 10 μL of CCK-8 reagent (Solarbio, Beijing, China) were incorporated at 0, 24, 48, and 72 h, respectively. Cells were incubated for 2 h at 37 °C, followed by measurement of absorbance at 450 nm using a microplate reader (DALB, Shanghai, China).

Wound healing assay

HCC cells were plated into each well of 24-well plates. Once cells were 90% confluent, a 200 μL pipette tip was used to scratch the cell monolayer, creating a consistent width. At 0 and 24 h, migratory cells were viewed in five randomly chosen fields under a light microscope (OLYMPUS, Tokyo, Japan). Wound widths were detected with ImageJ software (National Institutes of Health, Bethesda, MD, USA). The ratio of wound healing was computed as follows: migration distance/initial intercellular distance × 100%.

Transwell assay

The ability of cell invasion was assessed by an invasion chamber precoated with Matrigel (8-mm pores; BD Biosciences, California, USA). In the upper chamber, 100 μL of cells with a concentration of 5×10^5 cells/mL were introduced, while the lower chamber was filled with 600 μL of medium supplemented with 20% FBS. Cells that invaded the Transwell membrane were fixed with 4% paraformaldehyde for 10 min and stained with 0.1% crystal violet for 20 min following a 48-h incubation at 37 °C. The stained cells were observed under a light microscope.

C-circles (CC) assay

The C-circle assay was conducted according to previously reported methods [18]. Briefly, genomic DNA was isolated using the PureLink Genomic DNA Mini Kit (K182001; Thermo Fisher Scientific). Genomic DNA (250 ng) was digested with 0.25 μL of HinfI and 0.25 μL of RsaI (4 U/μg) at 37 °C for 4 h, followed by dilution to the specified concentrations of 25, 50, or 100 ng per 10

μL. Different concentrations of genomic DNA were combined in a 10 μL of reaction mixture, containing 5 μg BSA, 1 mM dATP, 1 mM dTTP, 1 mM dGTP, Φ29 buffer, and 5 U Φ29 DNA polymerase (NEB). Samples were incubated at 30 °C for 8 h followed by 20 min at 65 °C. The final reaction product or input DNA was slot-blotted onto a 2×SSC-soaked Hybond-N+membrane. The membrane was UV crosslinked and then hybridized at 45 °C using 5′-labeled TelC probes for Φ29 DNA polymerase amplified products or Alu probes for input DNA. TeloC probe: 5′-Biotin-CCCTAACCCTAACCCTAA-3′; Alu probe: 5′-Biotin-GGCCGGGCGCGGTGGCTCACGCCTGTAATCCCAGCA-3′.

Statistical analysis

In the bioinformatic analysis, all data were analyzed using R software (version 4.1.2). To estimate relationships between variables that are not linearly related, the Spearman correlation test was used. The Student's t-test compared normally distributed data. The chi-square test was used to compare categorical and pairwise features of subgroups. The Wilcoxon test was employed for comparing ordinal and non-normally distributed data between subgroups. For one independent variable with multiple levels and an ordinal dependent variable, the Kruskal-Wallis test was applied. Data from cellular experiments were processed using GraphPad Prism 7.0 software. The data were expressed as means±SD from minimum three replicates. Student's t-test was used for evaluating differences between two groups, while ANOVA with Tukey's test was employed for multiple-group comparisons. Unless specified otherwise, statistical significance was defined as a two-tailed $p<0.05$.

Results

Combined and calibrated GEO datasets

First, we merged the three validated HCC datasets, including GSE25097, GSE46408, and GSE84402, which were obtained from the GEO database. The batch effect was removed with the sva package in the R software for the three datasets. The combined GEO datasets were then normalized (Fig. 1A and B), and the results showed that the batch effect was largely eliminated for samples from different sources. Moreover, principal component analysis (PCA) of the expression matrices before and after the removal of the batch effect further verified the effectiveness of the batch effect elimination (Fig. 1C and D). The combined GEO dataset included 288 cases of HCC and 263 normal control samples.

Identification of DEGs in the TCGA database for LIHC

Subsequently, we downloaded LIHC-related transcriptome data in the TCGA database. DEGs in LIHC in the TCGA database were identified based on |logFC| > 0 and $p<0.05$. Consequently, 13,305 DEGs were screened, of which 10,414 were highly expressed and 2,891 DEGs were lowly expressed, and the volcano map of these DEGs were plotted (Fig. 2A). The intersection of the obtained DEGs and ALTRGs were taken to identify ALTRDEGs associated with LIHC, resulting in 500 ALTRDEGs (Fig. 2B). Moreover, the difference ordering of ALTRDEGs was also analyzed (Fig. 2C).

GO and KEGG enrichment analysis of ALTRDEGs

The potential biological functions of 500 ALTRDEGs were investigated by GO and KEGG enrichment analysis. The findings indicated that the 500 ALTRDEGs were primarily abundant in BP such as the regulation of DNA metabolic processes, double-strand break repair, telomere organization, and DNA recombination. In terms of CC, ALTRDEGs were significantly correlated with the chromosomal region, chromosome, telomeric region, nuclear chromosome, and protein-DNA complex. For MF, ALTRDEGs were strongly related to catalytic activity acting on DNA, DNA-binding transcription factor binding, RNA polymerase II-specific DNA-binding transcription factor binding, and ATP-dependent activity. Meanwhile, KEGG showed that ALTRDEGs were mostly engaged in biological pathways, including alcoholism, neutrophil extracellular trap formation, viral carcinogenesis, DNA replication, and cell cycle (Fig. 3A and F; Supplementary Table 4).

GSEA and GSVA of ALTRDEGs

The biological processes of genes in the TCGA-LIHC dataset were investigated by GSEA analysis (Fig. 4A and Supplementary Table 5), and the data revealed that genes in TCGA-LIHC were significantly enriched in the TP53 (Fig. 4B), Notch (Fig. 4C), Wnt (Fig. 4D), Jak Stat (Fig. 4E), and the Pi3k Akt pathways (Fig. 4F). GSVA results demonstrated that DNA repair, TNF-α signaling via NF-kB, xenobiotic metabolism, inflammatory response, and MYC targets were substantially different between the normal and LIHC groups (Fig. 4G; Supplementary Table 6).

Establishment of the risk model

To construct a risk model, we first conducted a univariate Cox regression analysis and variables with a $p<0.01$ were subsequently included in the LASSO regression analysis (Supplementary Fig. 2A-2B). Then, a multivariate Cox regression analysis was conducted and the results showed that there were 13 ALTRDEGs, including CDCA8, SMG5, RAD54B, FOXD2, NOL10, RRP12, CCT5, CCT4, HDAC1, DDX1, HRG, HDAC2, and PPP1CB could serve as independent prognostic biomarkers for LIHC (Supplementary Fig. 2C and Supplementary Table 7). Nomograms facilitated the quantitative prediction of patient

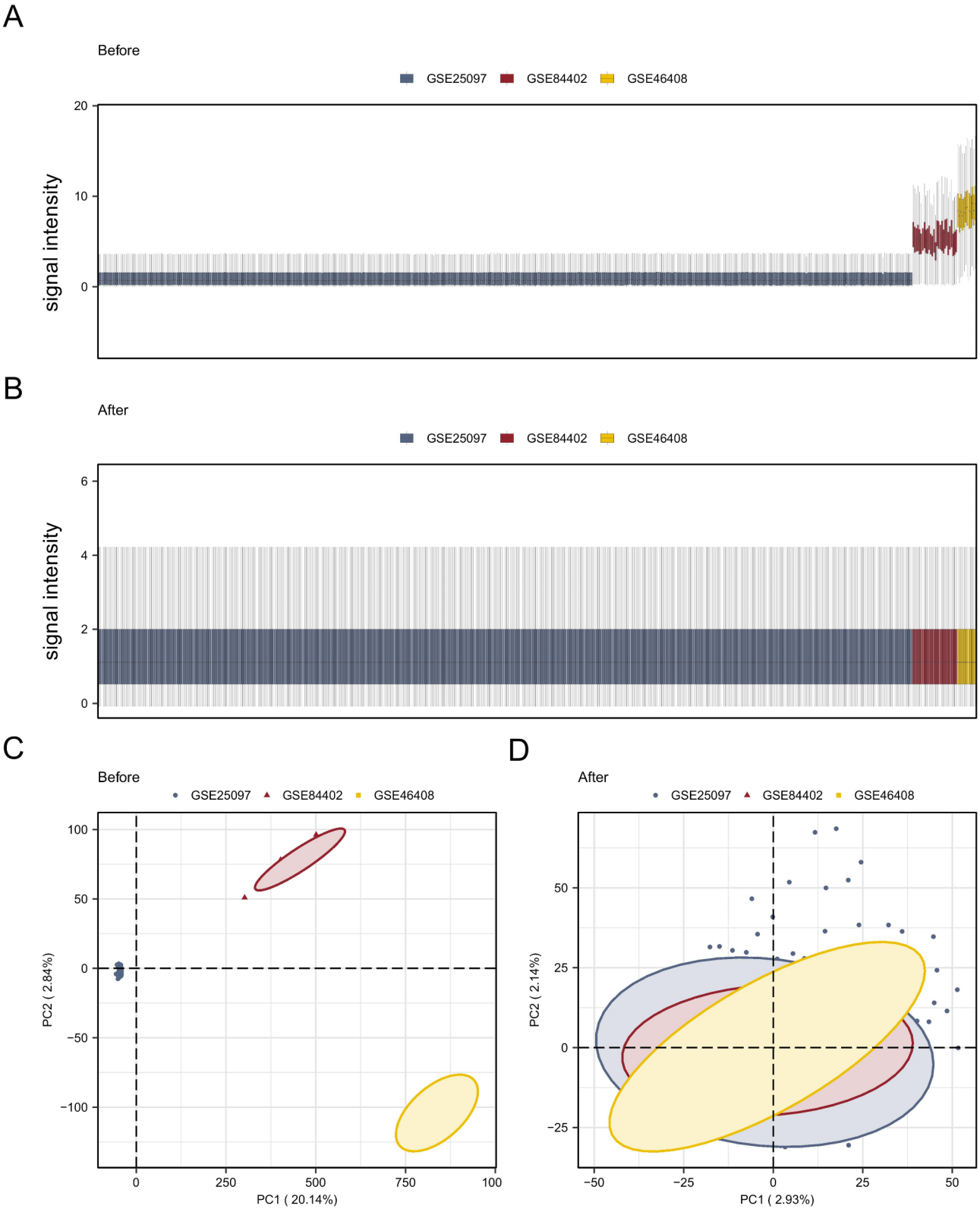

Fig. 1 The HCC datasets GSE25097, GSE46408, and GSE84402 were processed and corrected. **A**-**B**. Boxplot of the integrated GEO datasets before (**A**) and after (**B**) the normalization process. **C**-**D**. PCA plots of the combined GEO datasets before (**C**) and after (**D**) batch effect removal treatment. Blue color represents GSE25097 dataset, red color represents GSE84402 dataset, and yellow color represents GSE46408 dataset. HCC: hepatocellular carcinoma; PCA: principal component analysis

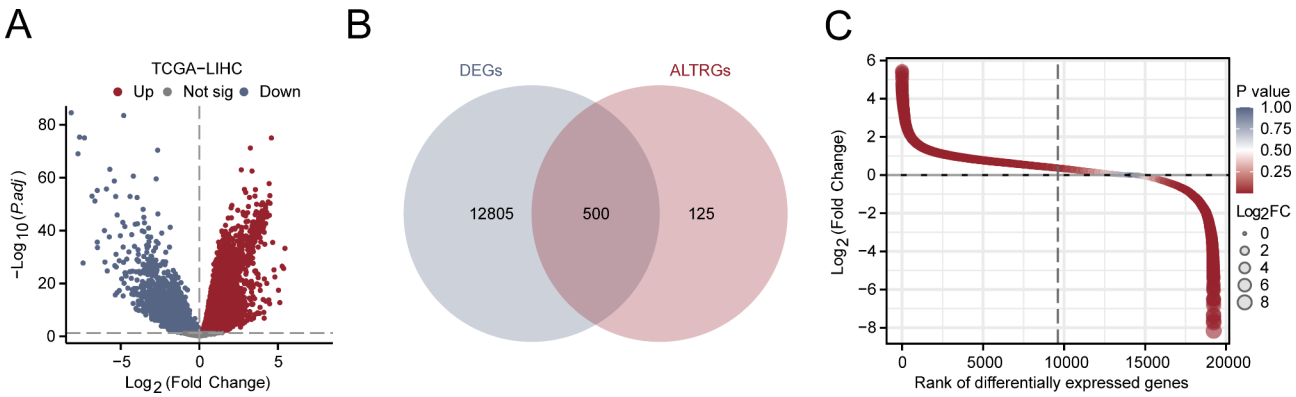

Fig. 2 Screening of LIHC-related DEGs. **A**. Volcano plot of DEGs in the LIHC and normal groups in the dataset TCGA-LIHC. **B**. Venn diagram showing ALTRDEGs. **C**. ALTRDEGs in the TCGA-LIHC dataset were ranked according to their p value and |logFC| value. HCC: liver hepatocellular carcinoma; DEGs: differentially expressed genes; ALTRGs: alternative lengthening of telomeres-related genes; ALTRDEGs: alternative lengthening of telomeres- related differentially expressed genes

prognosis, offering clinicians a reference point for making clinical decisions. The nomogram illustrated that SMG5 made the greatest contribution to the prognosis more than other ALTRDEGs (Supplementary Fig. 2D). Then, we performed 1-year, 3-year, and 5-year prognostic analyses and plotted calibration curves, which showed that the risk model predictions of patient survival were in general agreement with the actual patient survival (Supplementary Fig. 3A-3 C). Decision curve analysis (DCA) was used to assess the clinical efficacy of the risk model at 1-year (Supplementary Fig. 3D), 3-years (Supplementary Fig. 3E), and 4-years (Supplementary Fig. 3F). The findings demonstrated that the clinical utility of the 5-year prognostic model was greater than that of the 3-year prognostic model, which in turn was greater than that of the 1-year prognostic model.

Validation of prognosis-associated risk model

Survival curves for OS demonstrated poorer OS in the high-risk group compared to the low-risk group (Supplementary Fig. 4A). Additionally, the results showed that the risk score was significantly higher in the death group than in the survival group, suggesting a significant association between the high-risk scores and high probability of death (Supplementary Fig. 4B). As shown by the time-dependent AUC curve, risks score demonstrated moderate predictive validity for HCC onset at 1-, 3-, and 5-years ($0.7 < AUC < 0.9$; (Supplementary Fig. 4C-4D).

Expression and ROC curve analysis of prognostic ALTRDEGs in the TCGA-LIHC and GEO datasets

Based on the TCGA-LIHC and combined GEO datasets, the expressions of prognostic genes, including CDCA8, SMG5, RAD54B, FOXD2, NOL10, RRP12, CCT5, CCT4, HDAC1, DDX1, HDAC2, and PPP1CB were elevated in LIHC, whereas the expression of HRG was decreased in comparison to the normal group (Figs. 5A and 6A). According to the ROC curves in the TCGA-LIHC datasets, CDCA8, SMG5, NOL10, RAD54B, CCT5, CCT4, and DDX1 exhibited an AUC over 0.9, reflecting a high predictive value for LIHC. FOXD2, RRP12, HDAC1, HDAC2, PPP1CB, and HRG had an AUC ranging from 0.7 to 0.9, indicating moderate predictive accuracy for LIHC (Fig. 5C and N). At the same time, according to the ROC curves in the combined GEO dataset, CDCA8 had an AUC over 0.9. SMG5, FOXD2, RAD54B, HDAC1, CCT5, DDX1, and CCT4 showed an AUC from 0.7 to 0.9, while NOL10, HRG, HDAC2, and RRP12 had an AUC between 0.5 and 0.7 (Fig. 6B and N).

Exploration of CNV and SM for prognostic genes

Based on the LIHC-TCGA dataset, we performed somatic mutation and CNV analysis on 13 prognostic genes. The results indicated that the predominant mutations in these genes were missense mutations, primarily in the form of SNPs. The most common single nucleotide variants SNVs observed in LIHC were C to A mutations (Supplementary Fig. 5A). These 13 prognostic genes were then ranked and visualized according to their mutation frequency, from high to low (Supplementary Fig. 5B). Additionally, CNV analysis using GISTIC 2.0 revealed significant numbers of amplifications and deletions among the 13 prognostic genes in LIHC samples. SMG5, RAD54B and CCT5 had relatively high amplification frequencies. On the contrary, the deletion frequencies of HDAC1, HDAC2 and CDCA8 were relatively high (Supplementary Fig. 5C).

Prognostication of immunotherapy response with the ALTs-score model

The scores of ALTs were calculated based on ssGSEA algorithm and HCC patients were categorized into high and low groups according to the score. The IPS associated with LIHC from the TCGA database was downloaded to

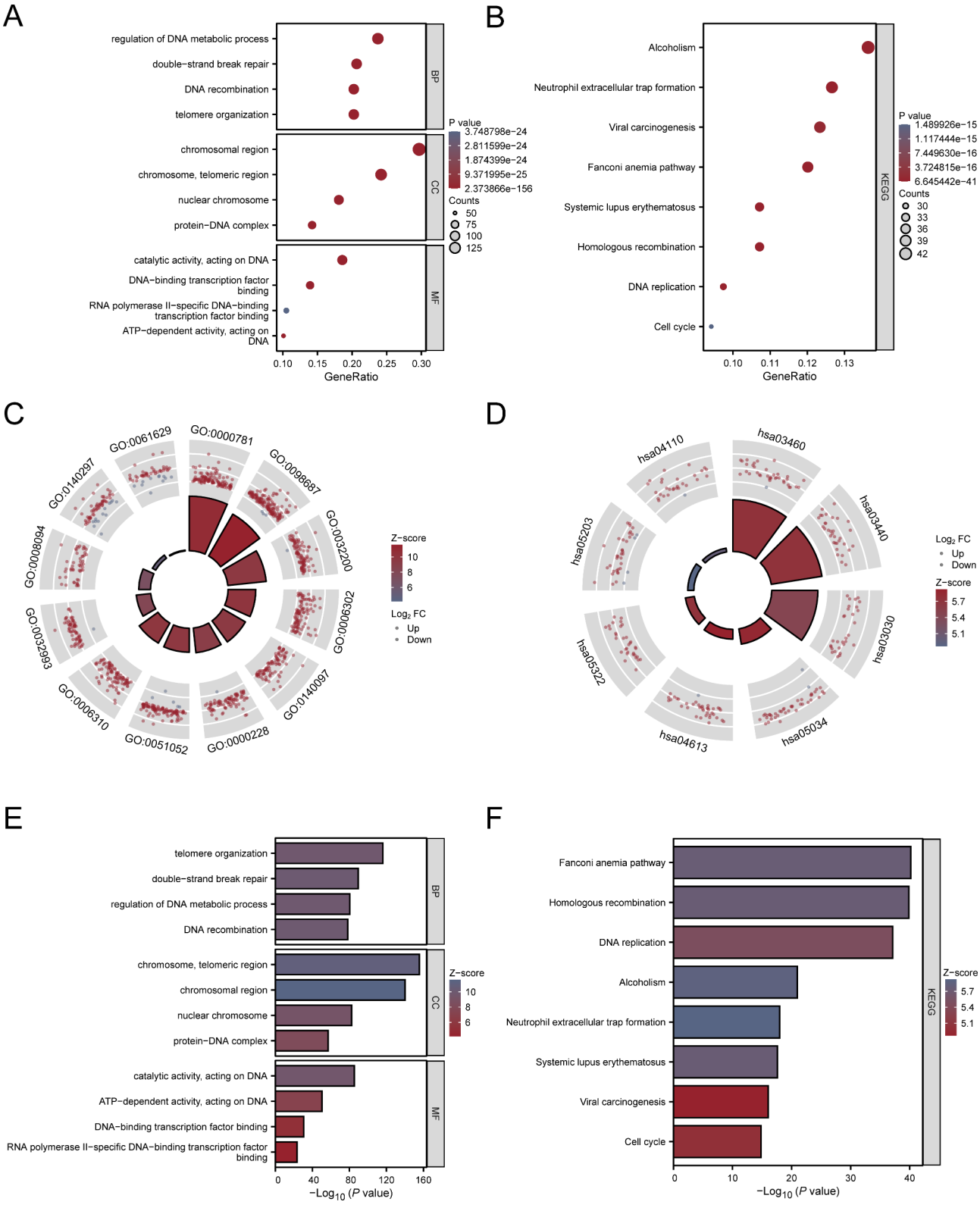

Fig. 3 (See legend on next page.)

(See figure on previous page.)

Fig. 3 GO and KEGG enrichment analysis for ALTRDEGs. **A**-**B**. Bubble plots of GO and KEGG enrichment analysis results for ALTRDEGs. The analysis included BP, CC, MF, and KEGG. In the bubble diagrams, the size of each bubble represents the number of genes, and the color of the bubbles indicates the p value size. Redder colors denote smaller p values, while bluer colors indicate larger p values. **C**-**D**. Circle plots of GO and KEGG enrichment analysis results for ALTRDEGs. The outer circle in each plot displays the molecules and their |logFC| values, with red indicating up-regulated genes and blue indicating down-regulated genes. A positive z-score suggests positive regulation, while a negative z-score suggests negative regulation. The larger the absolute value of the z-score, the higher the degree of regulation. **E**-**F**. Histograms of the results of GO and KEGG enrichment analysis of ALTRDEGs. Vertical coordinates represent GO terms or KEGG terms. The screening criteria for GO and KEGG enrichment analysis were $p < 0.05$ and FDR < 0.05. ALTRDEGs: alternative lengthening of telomeres-related differentially expressed genes; GO: Gene Ontology; KEGG: Kyoto Encyclopedia of Genes and Genomes; BP: biological process; CC: cellular component; MF: molecular function

explore the prediction of immunotherapy efficacy using the telomerase selective prolongation score model. The results revealed that the low group had higher IPS scores than high group in all categories, including IPS (Supplementary Fig. 6A), IPS-PD1/PD-L1/PD-L (Supplementary Fig. 6B), IPS-CTLA4 (Supplementary Fig. 6C), and IPS-PD1/PD-L1/PD-L2+CTLA4 (Supplementary Fig. 6D), suggesting that ALTs-score model could be predictive of the prognosis of immunotherapy.

Evaluation of immune cell distribution

The analysis of immune infiltration demonstrated that 13 immune cells were significantly associated with the ALTs-score (Supplementary Fig. 7A-7B). Additionally, there were positive correlations between SMG5 and immune cell M0 macrophage, as well as between RRP12 and immune cell M0 macrophage (Supplementary Fig. 7C). There were positive correlations between monocytes and resting mast cells, and between M0 macrophage and regulatory T cell (Treg). In contrast, negative correlations were observed between T follicular helper cell (Tfh) and resting CD4+memory T cells, and between resting mast cells and T follicular helper cell (Tfh) (Supplementary Fig. 7D).

Construction of LIHC subtypes

Using consistent clustering, LIHC patients were categorized into various subgroups based on the 13 ALTRDEGs expressions. CMplots were then employed to visualize the matrix heatmap at k=2, showing clear distinctions between the two clusters (Supplementary Fig. 8A). LIHC subtype 1 (cluster1) included 115 samples and LIHC subtype 2 (cluster2) comprised 259 samples. PCA revealed significant differences between the cluster1and cluster2 samples (Supplementary Fig. 8B). The empirical cumulative distribution attained its greatest approximation at k=2, thus indicating maximum stability (Supplementary Fig. 8C-8D). Furthermore, there were significant differences in the expression of all 13 hub genes between cluster1 and cluster2 (Supplementary Fig. 8E).

Assessment of the prognostic value of the ALTs-score model

In the nomogram, predictive factors included the ALTs model along with other clinicopathological features. The combined nomogram indicated that the T stage and ALTs-score model had the high weights among all the clinically relevant covariates (Supplementary Fig. 9A; Supplementary Table 8). Similarly, multivariate Cox analysis revealed that the ALTs-score model (HR: 0.419, 95% CI: 0.254–0.693, $p<0.001$), T2 stage (HR: 0.457, 95% CI: 0.237–0.882, $p=0.020$), and T1 stage (HR: 0.280, 95% CI: 0.157–0.501, $p<0.001$) were independent prognostic factors for HCC patients (Supplementary Fig. 9B). According to the calibration curves, the predicted OS values were consistent with the actual outcomes (Supplementary Fig. 9C-9E). CA curves demonstrated that the clinical utility of the 5-year ALTs-score model was superior to that of the 3-year ALTs-score model, which, in turn, was superior to the 1-year ALTs-score (Supplementary Fig. 9F-9 H).

RT-qPCR detection of mRNA expression levels of prognostic ALTDEGs

The mRNA expression levels of eight prognostic ALTDEGs with AUC>0.7 were verified by RT-qPCR in human normal hepatocytes L-02 and human HCC cells (SK-HEP-1 and SNU-387). The findings revealed that the expression levels of CDCA8, SMG5, RAD54B, FOXD2, CCT5, CCT4, HDAC1, and DDX1 were significantly increased in SK-HEP-1 and SNU-387 cells compared with the L-02 cells (Fig. 7).

Silencing of SMG5 inhibited HCC cell proliferation, migration, and invasion

According to the nomogram, SMG5 had a greater impact on the prognosis than any other ALTRDEGs (Supplementary Fig. 2D). Moreover, previous research has suggested that SMG5 may be an important target for immunotherapy of HCC [19]; therefore, we chose SMG5 for in-depth exploration. SMG5 expression was knocked down both in SK-HEP-1 and SNU-387 cells. RT-qPCR and western blot showed that there was no significant difference of SMG5 expression between the si-NC and Control groups in the two types of HCC cells. The expression of SMG5 in the si-SMG5-1, si-SMG5-2, and si-SMG5-3 groups was notably lower than that in the si-NC group both at mRNA and protein levels. Among these, si-SMG5-1 exhibited the best knockdown efficiency in both cell types and was therefore selected for

subsequent experiments (Fig. 8A and B). CCK-8 assay showed that SMG5 silencing suppressed SK-HEP-1 and SNU-387 cell proliferation (Fig. 8C). The migration and invasion capabilities of SK-HEP-1 and SNU-387 cells were assessed using wound healing and Transwell assays. The data indicated that the migration and invasive ability of HCC cells were markedly reduced after SMG5 silencing (Fig. 8D and E).

Silencing of SMG5 reduced the C-circle level of ALT cells

C-circles, which are circular DNA structures derived from telomeric repeats, are frequently used as indicators of ALT activity [20]. We subsequently measured C-circle level in SNU-387 cells following SMG5 silencing. We found that silencing of SMG5 notably decreased the C-circle level (Fig. 9).

Discussion

HCC is one of the most challenging cancers globally, with the characteristics of high morbidity and mortality [21]. Each year, nearly seven million people are diagnosed with HCC, and the disease causes over six million deaths [22]. Despite improvements in HCC therapy in recent years, the prognosis for HCC patients continues to be poor due to malignant infiltration and metastasis [23]. Thus, it is important to identify reliable and effective prognostic biomarkers and prospective therapeutic targets for HCC. In this study, we identified 13 prognostic genes. Upon construction and validation, the risk model, ALTs-score model, and visual nomogram performed with remarkable predictive accuracy, calibration, and applicability. Moreover, we found that silencing of SMG5 inhibited the proliferation, migration, and invasion of HCC cells. SMG5 silencing also reduced C-circle level in HCC cells.

The telomerase-independent ALT pathway was initially discovered in the *S. cerevisiae* telomerase mutant and later delineated in human cancer cell lines and tumors [24]. Lagging strand synthesis encounters the end replication problem, which prevents complete replication of the 5' end and contributes to the gradual shortening of chromosomal ends with successive cell divisions [25]. To counteract telomere depletion and evade replicative senescence, certain cancerous cells utilize the ALT pathway to lengthen telomeres and sustain their proliferative potential [26]. ALT + cancers can be identified by various methods, such as fluorescence in situ hybridization (FISH), which serves as a diagnostic and prognostic tool for these cancers. In oligodendrogliomas, ALT correlates with shorter progression-free survival and is an independent prognostic indicator [27]. ALT FISH status determined by immunohistochemistry can distinguish indolent cases from aggressive small low-grade pancreatic neuroendocrine tumors, and identify those patients who might benefit more from surgical intervention [28]. Furthermore, ALT is a predictor of the site of origin in neuroendocrine tumor liver metastases, particularly useful in identifying the primary tumor when its origin is unclear [29]. Another study has shown that ALT positivity is a strong risk predictor, especially in non-insulinomas. Patients with ALT-positive pancreatic neuroendocrine tumors generally have significantly shorter progression-free survival compared to those with ALT-negative in a Chinese cohort [30]. ALT in pediatric high-grade gliomas can occur independently of ATRX mutations and is commonly found in patients with pathogenic germline mismatch repair variants [31]. These findings indicate that ALT has important applications in clinical practice. Increasing number of studies have shown that ALT plays a role in HCC. A previous study found that 11 out of 13 chromophobe HCC with abrupt anaplasia were ALT-positive, which suggests that chromophobe HCC with abrupt anaplasia are highly enriched in the ALT phenotype [32]. The types of ALT-positive primary hepatic epithelial tumors expand to include cholangiocarcinoma, HCC-cholangiocarcinoma comorbidities, and carcinosarcomas [33]. Furthermore, many studies are focused on understanding the clinical relevance of ALT in liver tumors. A preclinical study showed that hepatic angiosarcomas frequently exhibit the ALT phenotype, which is strongly correlated with the loss of ATRX expression [34]. ALT serves as a valuable biomarker in neuroendocrine tumor liver metastases patients and can identify the primary site in cases where it is unknown according to a tissue microarrays study [29]. The frequency of ALT positivity in chromophobe HCC is similar in men and women, unlike the male predominance observed in regular HCC patients [35]. G2/M checkpoint depressors have been designed for the treatment of ALT-positive cancers [36]. The above findings suggest that ALT is a promising target for the treatment of liver tumors. In this study, we found a novel ALTDEGs constructed risk model and a ALT-score model that was effective in forecasting the prognosis of HCC.

In this study, 13 ALTDEGs (CDCA8, SMG5, RAD54B, FOXD2, NOL10, RRP12, CCT5, CCT4, HDAC1, DDX1, HRG, HDAC2, and PPP1CB) were identified to develop a prognostic signature according to the LASSO Cox regression analysis. This risk score was able to predict 1-, 3-, and 5-year survival in patients with HCC. ROC curve analysis showed that 13 ALTDEGs could effectively distinguish HCC samples from normal samples. CDCA8 and PPP1CB are associated with cell cycle regulation. CDCA8 facilitates tumor proliferation and predicts poor prognosis in HCC. CDCA8 silencing inhibits HCC growth and stem cell properties through ATF3 tumor suppressor restoration and AKT/β-catenin signaling inactivation [37–39]. The rs13025377 variant in PPP1CB is significantly linked to an increased risk

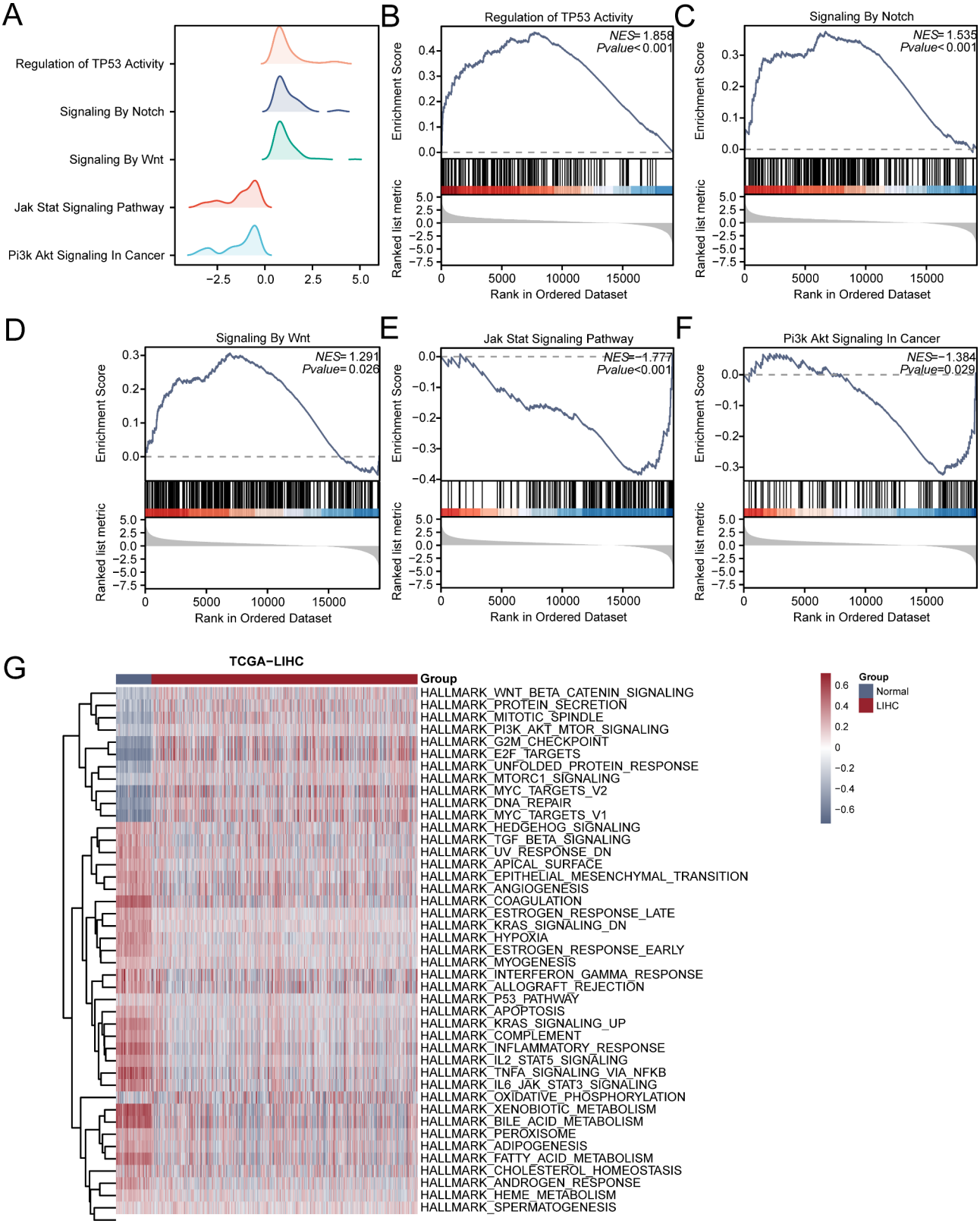

Fig. 4 GSEA and GSVA on the TCGA-LIHC dataset. **A**. Mountains map of five biological functions by GSEA of the dataset TCGA-LIHC. **B**-**F**. GSEA showed that all genes were significantly enriched in the TP53 pathway (**B**), Notch pathway (**C**), Wnt pathway (**D**), Jak Stat pathway (**E**), and the Pi3k Akt pathway (**F**). G. Heatmap of GSVA results between different subgroups (Normal/LIHC). The screening criteria for GSVA were $p < 0.05$ and FDR < 0.25. In the heatmap, blue indicates down-regulation and red indicates up-regulation. The LIHC group is represented in red, while the Normal group is represented in blue. TCGA: The Cancer Genome Atlas; LIHC: liver hepatocellular carcinoma; GSEA: Gene Set Enrichment Analysis; GSVA: Gene Set Variation Analysis

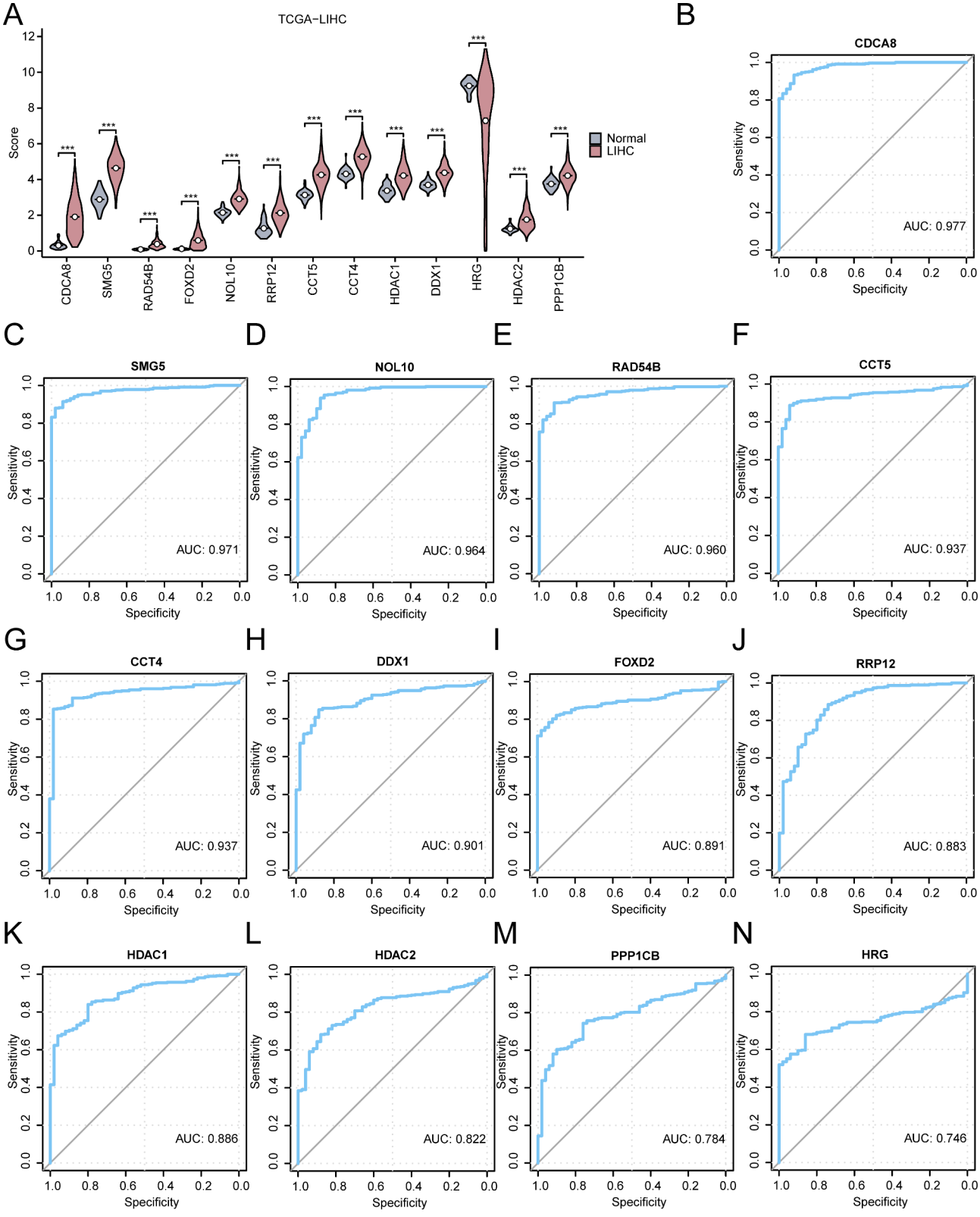

Fig. 5 Expression level and prognostic analysis of prognostic genes based on TCGA-LIHC dataset. **A**. Expression levels of prognostic genes in LIHC. Blue color represents the Normal group and red color represents the LIHC group. *** equivalent to $p < 0.001$. B-N. ROC curves for prognostic genes CDCA8 (**B**), SMG5 (**C**), NOL10 (**D**), RAD54B (**E**), CCT5 (**F**), CCT4 (**G**), DDX1 (**H**), FOXD2 (**I**), RRP12 (**J**), HDAC1 (**K**), HDAC2 (**L**), PPP1CB (**M**), and HRG (**N**). The closer the AUC in the ROC curve is to 1, the better the diagnostic effect. TCGA: The Cancer Genome Atlas; LIHC: liver hepatocellular carcinoma; ROC: receiver operating characteristic curve; AUC: area under curve

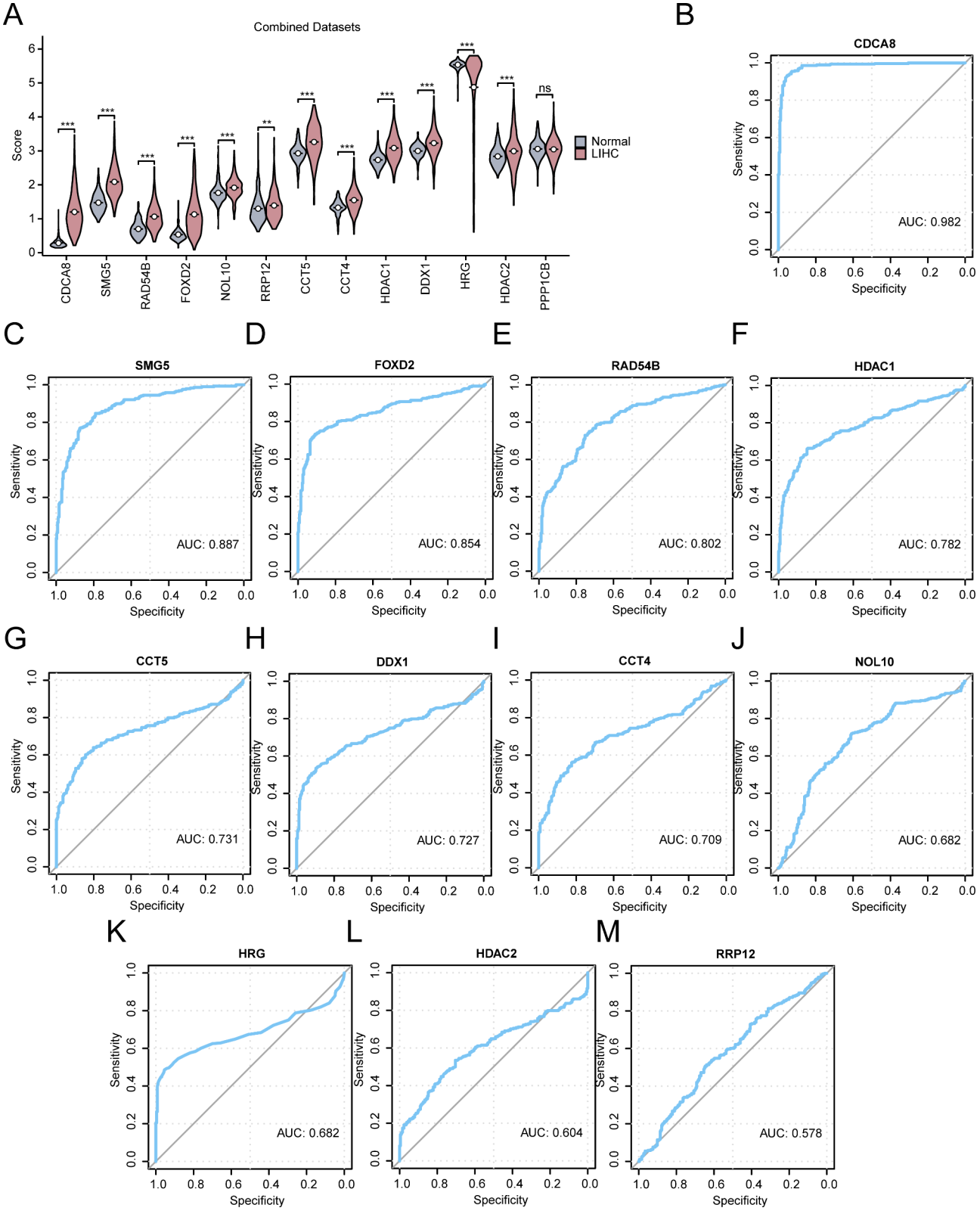

Fig. 6 Prognostic gene expression levels and ROC curve analysis were analyzed in the combined GEO dataset. **A**. Violin plot of expression levels of prognostic genes in LIHC. Blue color represents the Normal group and red color represents the LIHC group. *** indicates $p < 0.001$. **B**. ROC curves for prognostic genes CDCA8 (**B**), SMG5 (**C**), FOXD2 (**D**), RAD54B (**E**), HDAC1 (**F**), CCT5 (**G**), DDX1 (**H**), CCT4 (**I**), NOL10 (**J**), HRG (K), HDAC2 (**L**), and RRP12 (**M**) in the combined GEO dataset. The symbol ns corresponds to $p > 0.05$, indicating no significant difference, while *** corresponds to $p < 0.001$. TCGA: The Cancer Genome Atlas; LIHC: liver hepatocellular carcinoma; ROC: receiver operating characteristic curve; AUC: area under curve

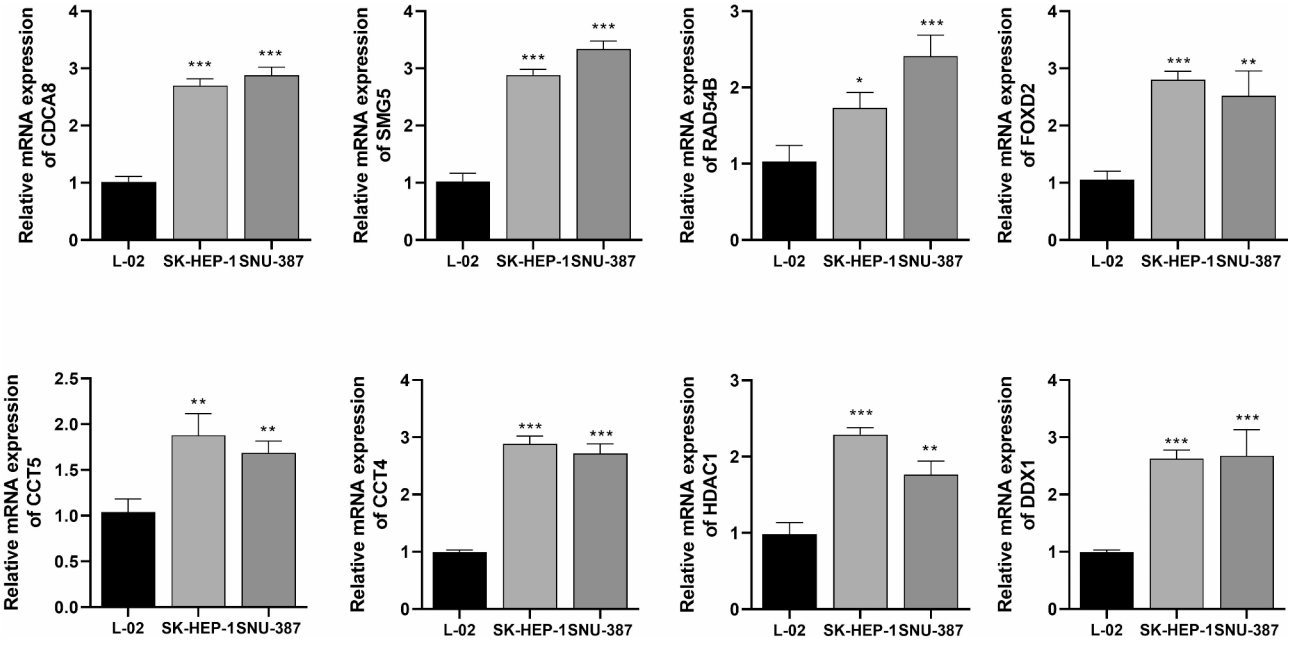

Fig. 7 Prognosis-related mRNA expression levels of ALTRGs (AUC > 0.7) were examined by RT-qPCR, including CDCA8, SMG5, RAD54B, FOXD2, CCT5, CCT4, HDAC1, and DDX1. $^{*}p < 0.05$, $^{*}p < 0.01$, $^{***}p < 0.001$ vs. L-02 group

of HBV-related HCC [40]. In this study, we found that CDCA8 was highly expressed in SK-HEP-1 and SNU-387 cells, suggesting that it might act as an oncogene in HCC. RAD54B is involved in the DNA repair process. RAD54B expression is elevated in HCC, which is consistent with our results. It fosters the development of HCC through the homologous recombination repair pathway or Wnt/β-catenin signaling activation [41, 42]. FOXD2, HDAC1, HDAC2 are all associated with transcriptional regulation. Dysregulation of the LncRNA FOXD2 adjacent opposite strand RNA 1 (FOXD2-AS1) facilitates the progression of a variety of tumors, such as glioma, retinoblastoma, and HCC [43–45]. Upregulation of HDAC1 and HDAC2 is significantly associated with a poorer prognosis of HCC patients, while their combined knockdown result in enhanced HCC cell death, reduce cell proliferation and colony formation [46, 47]. This study also showed that FOXD2 and HDAC1 mRNA levels were elevated in HCC cells, which might promote HCC progression. Ribosome biogenesis-related genes NOL10 and RRP12 have been reported to be independent prognostic factors for HCC [48, 49]. Study have shown that unfolded protein response-related genes CCT5 and CCT4 expression levels are significantly increased in HCC tissues at both transcript and protein levels. The present study further confirmed that the mRNA levels of CCT5 and CCT4 were elevated in SK-HEP-1 and SNU-387 cells. Moreover, high expression of CCT5 and CCT4 correlates with poor prognosis in HCC [50, 51]. DDX1 is engaged in RNA processing and HRG is associated with immune response, both of which serve as independent prognostic factors for HCC and are correlated with immune infiltration [52, 53]. DDX1 is highly expressed in HCC tissues and HCC cell lines, including SMMC-7721, QGY-7703 and HepG2. Similarly, our study showed that DDX1 expression was increased in SK-HEP-1 and SNU-387 cells. In this study, we found that these genes could be used as diagnostic biomarkers in addition to prognostic markers for HCC. Additionally, multiple studies have shown that 13 hub genes are involved in the progression of a variety of tumors, such as CDCA8 in prostate cancer [54], RAD54B in breast cancer [55], and HRG in ovarian [56]. These studies suggest that 13 hub genes play important roles in the progression of various types of tumors, rather than being specific to the HCC. Therefore, constructing a risk model based on these 13 genes could provide a more comprehensive tool for both the diagnosis and prognosis of HCC.

SMG5 is an RNA-binding protein and contributes to mRNA degradation via the nonsense-mediated decay pathway [57]. Zhang et al. found that in pancreatic cancer, DDIT4-AS1, an oncogene, segregates SMG5 and PP2A from UPF1 and enhances nonsense-mediated decay by increasing UPF1 phosphorylation [58]. Furthermore, a pan-cancer analysis has revealed that SMG5 expression is elevated in 23 types of tumors and may serve as a risk gene for many of them, with particular significance for the prognosis and tumor microenvironment in low-grade glioma patients [59]. Another study has showed that SMG5 is highly expressed in male patients with gastric cancer and are significantly associated with poor patient prognosis [60]. Moreover, prognostic models based on

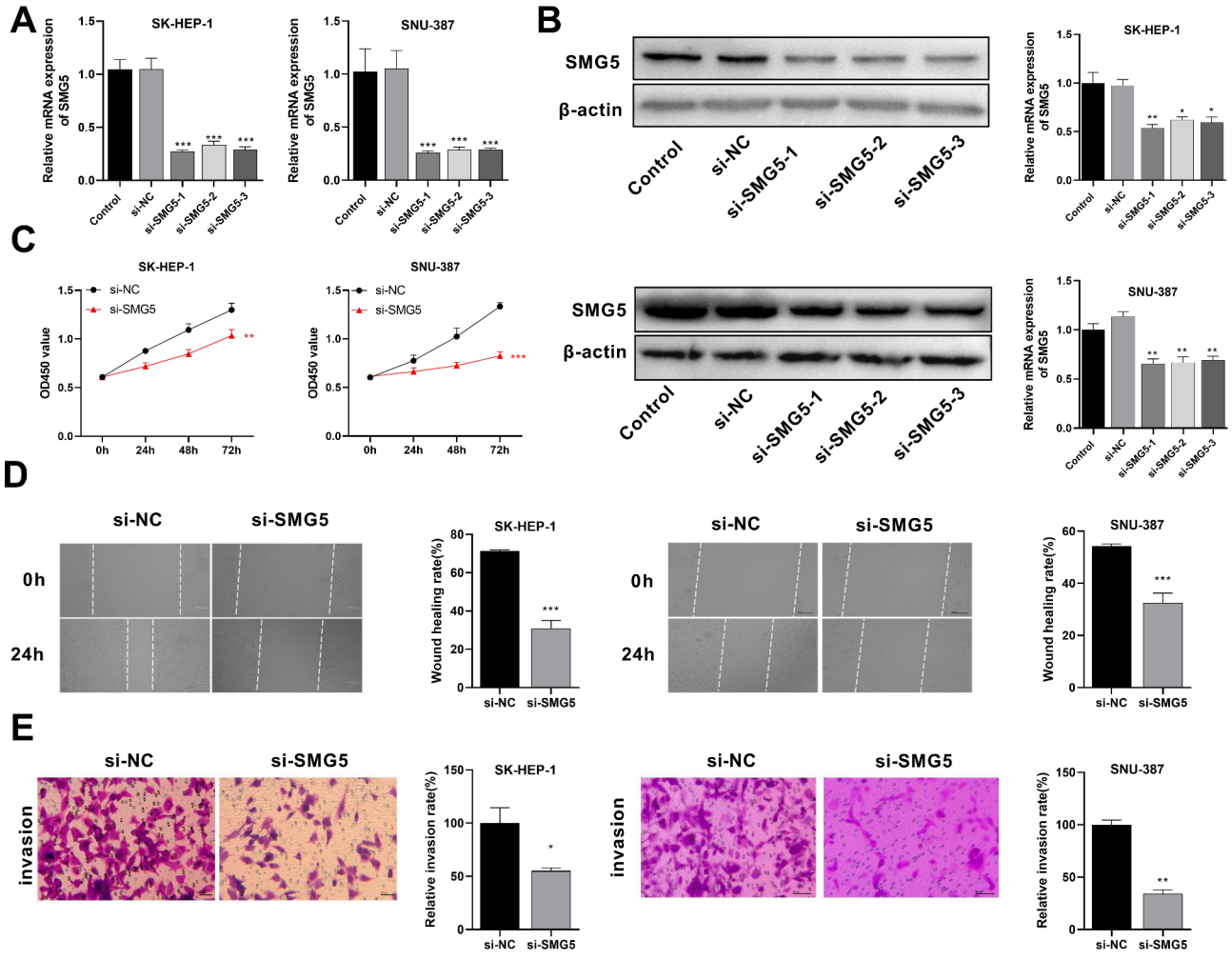

Fig. 8 Silencing of SMG5 inhibited HCC cell proliferation, migration, and invasion. **A**-**B**. SMG5 expression was knocked down using si-SMG5-1, si-SMG5-2, and si-SMG5-3 both in SK-HEP-1 and SNU-387 cells and transfection efficiencies were assessed by RT-qPCR and western blot. **C**. CCK-8 was used to measure HCC cell proliferation capacity in si-NC and si-SMG5 groups. **D**-**E**. The effects of SMG5 knockdown on HCC cell migration (**D**) and invasion (**E**) were assessed by wound healing assay and Transwell assay. $^{*}p < 0.05$, $^{**}p < 0.01$, $^{***}p < 0.001$ vs. si-NC group

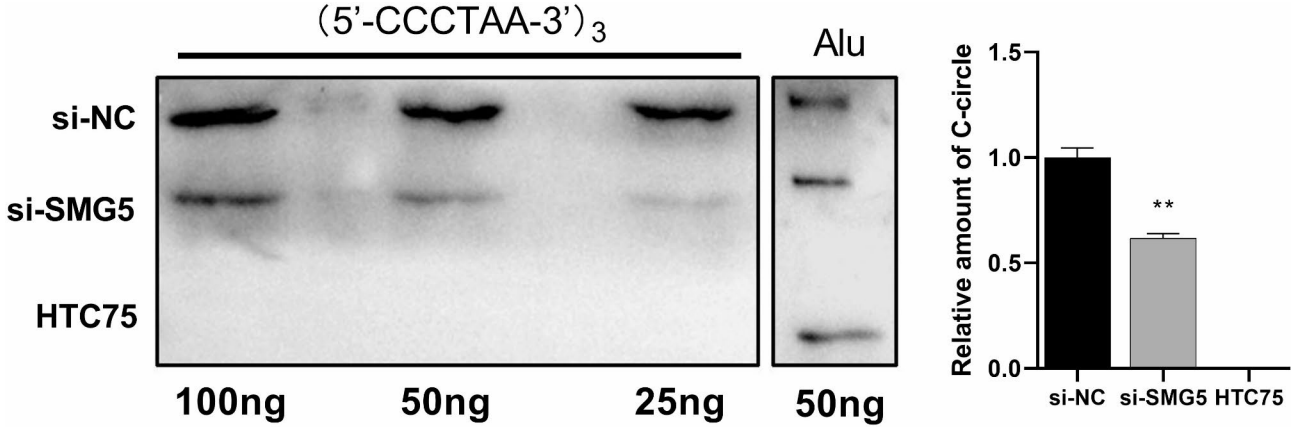

Fig. 9 C-circle assays were performed using SNU-387 genomic DNA (25, 50, or 100 ng) extracted from si-NC and si-SMG5 cells. $^{**}p < 0.01$ vs. si-NC group

SMG5 and other RNA-binding proteins could predict clinical outcomes in patients with HCC [61–63]. The overexpression of TMEM79 along with SMG5 is connected to unfavorable prognosis, tumor immune infiltration, and drug sensitivity in HCC [64]. It is also reported that SMG5 is linked to the immune cell infiltration, such as macrophages, B cells, and T cells, in HCC [65]. Similarly, in the present study, we found that upregulation of SMG5 signaled poor prognosis in HCC patients and there was a positive correlation between SMG5 and immune cell Macrophages M0. These studies indicate the potential of SMG5 as a negative prognostic marker for many tumor patient outcomes and it is a promising target for HCC treatment, especially in immunotherapy. Prior research indicates that knockdown of SMG5 inhibits the migration, invasion and proliferation of Hep3B and Huh7 cells, as well as augmented the response of HCC cells to sorafenib [66]. In our study, we further confirmed that SMG5 knockdown inhibited the proliferation, migration and invasion of SK-HEP-1 and SNU-387 cells lines, suggesting that SMG5 might function as an oncogene in HCC. Additionally, the role of SMG5 in other tumors remains poorly understood, which require extensive further research to fully understand the underlying roles of SMG5 in tumors. The CC assay has emerged as a frontline method for investigating the ALT mechanism [67]. The C-circle level provides valuable diagnostic value for various tumors, such as sarcomas and gliomas [68, 69]. This study revealed that silencing SMG5 decreased C-circle levels in HCC cells, suggesting that SMG5 is involved in the ALT mechanism in HCC. However, there were some limitations to this study. First, the study pinpointed 13 key ALT-related genes in HCC. Although we acknowledged the importance of other genes, such as HRG, we were focusing on SMG5 due to time and resource constraints. In future studies, we will consider validating other important genes in HCC. Second, this study focused mainly on the effects of SMG5 knockdown on HCC development. The impact of SMG5 overexpression and knockout mediated by CRISPR-Cas9 on HCC progression still needs to be explored in our future research, gaining a more comprehensive understanding the role of SMG5 in HCC. Then, the conclusions drawn from this study were based on in vitro experiments. In vivo and clinical studies are necessary next steps to validate these findings and further explore the therapeutic potential of the identified targets in HCC.

Conclusion

We identified prognostic ALTDEGs and developed a prognostic ALTDEGs signature and an ALTs-score model in HCC. Furthermore, SMG5 silencing suppressed the proliferation, migration, and invasion of SK-HEP-1 and SNU-387 cells. This study provides new biomarkers for predict the prognosis of HCC and potential targets for HCC treatment.

Supplementary Information

The online version contains supplementary material available at https://doi.org/10.1186/s12885-024-13146-0.

Supplementary Material 1

Acknowledgements

Not applicable.

Author contributions

Study concept and design: FLZ&YLC. Data acquisition: JL. Data analysis and interpretation: JL. Drafting of the manuscript: FLZ&YLC; critical revision of the manuscript for important intellectual content: FLZ&YLC. Statistical analysis: JL. Obtained funding: FLZ&YLC. Administrative, technical, or material support: FLZ&YLC; study supervision: JL.

Funding

Not applicable.

Data availability

The data that support the findings of this study are openly available in Gene Expression Omnibus at https://www.ncbi.nlm.nih.gov/geo/, reference number GSE25097 (GPL6947 platform), GSE46408 (GPL4133 platform), and GSE84402 (GPL570 platform) .

Declarations

Ethics approval and consent to participate

All animal experiments were approved by The First Affiliated Hospital of Gannan Medical University (No. 22SC-2024-191) in accordance with ARRIVE Guidelines.

Consent for publication

Not applicable.

Competing interests

The authors declare no competing interests.

Author details

[1]Department of General Surgery (Hepatobiliary and Pancreatic Surgery), The First Affiliated Hospital of Gannan Medical University, Ganzhou, China
[2]Department of Gastroenterology, The First Affiliated Hospital of Gannan Medical University, Ganzhou, China
[3]Department of Intensive Medicine (Comprehensive Intensive Care Unit), The First Affiliated Hospital of Gannan Medical University, No. 128 Jin Ling Lu, Ganzhou, Jiangxi 341000, P.R. China

Received: 26 July 2024 / Accepted: 4 November 2024
Published online: 11 November 2024

References

1. Sung H, et al. Global Cancer statistics 2020: GLOBOCAN estimates of incidence and Mortality Worldwide for 36 cancers in 185 countries. CA Cancer J Clin. 2021;71(3):209–49.
2. Vogel A, et al. Hepatocellular carcinoma. Lancet. 2022;400(10360):1345–62.
3. Hatzidakis A et al. Local and Regional therapies for Hepatocellular Carcinoma and Future combinations. Cancers (Basel), 2022. 14(10).
4. Peter M. L.J.B., *Telomeres, aging, and cancer: the big picture.* 2022. 139(6).
5. Jixuan G, Hilda PJNRC. A, *Targeting telomeres: advances in telomere maintenance mechanism-specific cancer therapies.* 2022. 22(9).
6. Loe TK, et al. Telomere length heterogeneity in ALT cells is maintained by PML-dependent localization of the BTR complex to telomeres. Genes Dev. 2020;34(9–10):650–62.

7. Emilie F et al. Length-dependent Process Telomeres Absence Telomerase 2014. 42(6).
8. Liu H, et al. Telomeric Recombination Induced by DNA damage results in Telomere extension and length heterogeneity. Neoplasia. 2018;20(9):905–16.
9. Mori JO, et al. Alternative lengthening of telomeres: mechanism and the pathogenesis of cancer. J Clin Pathol. 2024;77(2):82–6.
10. Yasir S, et al. Alternative lengthening of telomeres in primary hepatic neoplasms. Hum Pathol. 2023;131:79–86.
11. Lawlor RT, et al. Alternative lengthening of telomeres (ALT) influences survival in soft tissue sarcomas: a systematic review with meta-analysis. BMC Cancer. 2019;19(1):232.
12. Cai Y, et al. An alternative extension of telomeres related prognostic model to predict survival in lower grade glioma. J Cancer Res Clin Oncol. 2023;149(15):13575–89.
13. Peng Q et al. NFRKBNuclear factor related to KappaB binding protein () is a Telomere-Associated protein and involved in Liver Cancer Development. 2021. 40(10): pp. 1298–307.
14. Li S, Gao K, Yao D. Comprehensive Analysis of angiogenesis associated genes and tumor microenvironment infiltration characterization in cervical cancer. Heliyon. 2024;10(12):e33277.
15. Li X, et al. Deep-frying oil induces cytotoxicity, inflammation and apoptosis on intestinal epithelial cells. J Sci Food Agric. 2022;102(8):3160–8.
16. Kang J, et al. LASSO-Based machine learning algorithm for prediction of Lymph Node Metastasis in T1 colorectal Cancer. Cancer Res Treat. 2021;53(3):773–83.
17. Zheng H, et al. Characterization of stem cell landscape and identification of stemness-relevant prognostic gene signature to aid immunotherapy in colorectal cancer. Stem Cell Res Ther. 2022;13(1):244.
18. Wang C, Songyang Z, Huang Y. TRIM28 inhibits alternative lengthening of telomere phenotypes by protecting SETDB1 from degradation. Cell Biosci. 2021;11(1):149.
19. Yu W et al. Overexpression of TMEM79 combined with SMG5 is related to prognosis, tumor immune infiltration and drug sensitivity in hepatocellular carcinoma. 2023. 28(1).
20. Henson JD, et al. The C-Circle assay for alternative-lengthening-of-telomeres activity. Methods. 2017;114:74–84.
21. Llovet JM, et al. Hepatocellular carcinoma. Nat Rev Dis Primers. 2021;7(1):6.
22. Sagnelli E, et al. Epidemiological and etiological variations in hepatocellular carcinoma. Infection. 2020;48(1):7–17.
23. Xie M, et al. FGF19/FGFR4-mediated elevation of ETV4 facilitates hepatocellular carcinoma metastasis by upregulating PD-L1 and CCL2. J Hepatol. 2023;79(1):109–25.
24. Musmaker K et al. Alternative lengthening of telomeres in yeast: old questions and New approaches. Biomolecules, 2024. 14(1).
25. Cai SW, de Lange T. CST–Polα/Primase: the second telomere maintenance machine. Genes Dev. 2023;37(13–14):555–69.
26. Claude E, Decottignies A. Telomere maintenance mechanisms in cancer: telomerase, ALT or lack thereof. Curr Opin Genet Dev. 2020;60:1–8.
27. Zhi-Feng S et al. Alternative lengthening of telomeres is seen in a proportion of oligodendrogliomas and is associated with a worse prognosis. 2024. 6(1).
28. Neyaz A, et al. Predicting recurrence in pancreatic neuroendocrine tumours: role of ARX and alternative lengthening of telomeres (ALT). Histopathology. 2023;83(4):546–58.
29. Dogeas E, et al. Alternative lengthening of telomeres predicts site of origin in neuroendocrine tumor liver metastases. J Am Coll Surg. 2014;218(4):628–35.
30. Ban X, et al. Alternative lengthening of telomeres phenotype predicts progression risk in Noninsulinomas in a Chinese cohort. Neuroendocrinology. 2022;112(5):510–22.
31. Stundon JL, et al. Alternative lengthening of telomeres (ALT) in pediatric high-grade gliomas can occur without ATRX mutation and is enriched in patients with pathogenic germline mismatch repair (MMR) variants. Neuro Oncol. 2023;25(7):1331–42.
32. Kang HJ, et al. Clinicopathological and molecular characterization of chromophobe hepatocellular carcinoma. Liver Int. 2021;41(10):2499–510.
33. Tanaka A, et al. Proteogenomic characterization of primary colorectal cancer and metastatic progression identifies proteome-based subtypes and signatures. Cell Rep. 2024;43(2):113810.
34. Jau-Yu L et al. Alternative lengthening of telomeres phenotype in malignant vascular tumors is highly associated with loss of ATRX expression and is frequently observed in hepatic angiosarcomas. 2015. 46(9).
35. Wood LD, et al. Chromophobe hepatocellular carcinoma with abrupt anaplasia: a proposal for a new subtype of hepatocellular carcinoma with unique morphological and molecular features. Mod Pathol. 2013;26(12):1586–93.
36. Chen YJ, et al. Association of mutant TP53 with alternative lengthening of telomeres and favorable prognosis in glioma. Cancer Res. 2006;66(13):6473–6.
37. Cui Y, Jiang N. CDCA8 facilitates Tumor Proliferation and predicts a poor prognosis in Hepatocellular Carcinoma. Appl Biochem Biotechnol. 2024;196(3):1481–92.
38. Cui XH, et al. Cell division cycle associated 8: a novel diagnostic and prognostic biomarker for hepatocellular carcinoma. J Cell Mol Med. 2021;25(24):11097–112.
39. Jeon T et al. Silencing CDCA8 suppresses Hepatocellular Carcinoma Growth and Stemness via Restoration of ATF3 tumor suppressor and inactivation of AKT/beta-Catenin signaling. Cancers (Basel), 2021. 13(5).
40. Mai H, et al. A genetic variant of PPP1CB influences risk of Hepatitis B Virus-Related Hepatocellular Carcinoma in Han Chinese: a pathway based analysis. J Hepatocell Carcinoma. 2021;8:1055–64.
41. Li H, et al. RAD54L promotes progression of hepatocellular carcinoma via the homologous recombination repair pathway. Funct Integr Genomics. 2023;23(2):128.
42. Senwen F et al. *Amplification of RAD54B promotes progression of hepatocellular carcinoma via activating the Wnt/β-catenin signaling.* 2021. 14(8).
43. Zhao Q et al. LncRNA FOXD2-AS1 stimulates glioma progression through inhibiting P53. 2020. 24(8): pp. 4382–8.
44. Liang Y, et al. lncRNA FOXD2-AS1 promotes the Retinoblastoma Cell viability and Migration by sponging miR-31. Biomed Res Int. 2022;2022:p7723425.
45. Chen G, et al. LncRNA FOXD2-AS1 facilitates the progression of hepatocellular carcinoma by regulating TWIST1. Eur Rev Med Pharmacol Sci. 2023;27(10):4536–43.
46. Cai D, et al. Integrative analysis of lactylation-related genes and establishment of a novel prognostic signature for hepatocellular carcinoma. J Cancer Res Clin Oncol. 2023;149(13):11517–30.
47. Ler SY, et al. HDAC1 and HDAC2 independently predict mortality in hepatocellular carcinoma by a competing risk regression model in a southeast Asian population. Oncol Rep. 2015;34(5):2238–50.
48. Hu X, et al. Identification and validation of novel biomarkers for diagnosis and prognosis of Hepatocellular Carcinoma. Front Oncol. 2020;10:541479.
49. Wei C, et al. Validating RRP12 expression and its prognostic significance in HCC based on Data Mining and Bioinformatics methods. Front Oncol. 2022;12:812009.
50. Liheng Y, Xuejing Z, L.J.I.J.C.E P, Li. The TCP1 ring complex is associated with malignancy and poor prognosis in hepatocellular carcinoma. 2020. 12(9).
51. Zhang S, et al. Prognostic role of unfolded protein response-related genes in Hepatocellular Carcinoma. Curr Protein Pept Sci. 2023;24(8):666–83.
52. Mengping Y et al. DDX1 is a prognostic biomarker and correlates with immune infiltrations in hepatocellular carcinoma. 2022. 23(1).
53. Cai P et al. Molecular mechanism of aflatoxin-Induced Hepatocellular Carcinoma Derived from a Bioinformatics Analysis. Toxins (Basel), 2020. 12(3).
54. Wan S, et al. Overexpression of CDCA8 predicts poor prognosis and promotes Tumor Cell growth in prostate Cancer. Front Oncol. 2022;12:784183.
55. Zhang Z, et al. RAD54B potentiates tumor growth and predicts poor prognosis of patients with luminal A breast cancer. Biomed Pharmacother. 2019;118:109341.
56. Bakay K, et al. Effects of HRG and TP73 gene variations on ovarian response. Gynecol Endocrinol. 2022;38(3):243–7.
57. Boehm V, et al. SMG5-SMG7 authorize nonsense-mediated mRNA decay by enabling SMG6 endonucleolytic activity. Nat Commun. 2021;12(1):3965.
58. Zhang Y, et al. The m(6)a demethylase ALKBH5-mediated upregulation of DDIT4-AS1 maintains pancreatic cancer stemness and suppresses chemosensitivity by activating the mTOR pathway. Mol Cancer. 2022;21(1):174.
59. Yang L, et al. Pan-cancer Analysis of the prognostic and immunological role of SMG5: a biomarker for cancers. Oncology. 2024;102(2):168–82.
60. Li H, et al. Differences in the prognosis of gastric cancer patients of different sexes and races and the molecular mechanisms involved. Int J Oncol. 2019;55(5):1049–68.
61. Wang M, et al. Development and validation of an RNA binding protein-associated prognostic model for hepatocellular carcinoma. BMC Cancer. 2020;20(1):1136.
62. Man Z, et al. A prognostic model based on RNA binding protein predicts clinical outcomes in Hepatocellular Carcinoma patients. Front Oncol. 2020;10:613102.

63. Wang L, et al. Identification of an RNA binding protein-related gene signature in hepatocellular carcinoma patients. Mol Med. 2020;26(1):125.
64. Wang Y et al. Overexpression of TMEM79 combined with SMG5 is related to prognosis, tumor immune infiltration and drug sensitivity in hepatocellular carcinoma. 2023. 28(1): p. 490.
65. Bufu T et al. *Diagnosis and prognosis models for hepatocellular carcinoma patient's management based on tumor mutation burden.* 2021. 33(0).
66. Fang N, et al. SMG5 inhibition restrains Hepatocellular Carcinoma Growth and enhances Sorafenib Sensitivity. Mol Cancer Ther; 2024.
67. Jones CY, et al. Hyperextended telomeres promote formation of C-circle DNA in telomerase positive human cells. J Biol Chem. 2023;299(5):104665.
68. Burrow T et al. Prevalence of alternative lengthening of telomeres in pediatric sarcomas determined by the telomeric DNA C-circle assay. 2024. 14: p. 1399442.
69. Fogli A, et al. Detection of the alternative lengthening of telomeres pathway in malignant gliomas for improved molecular diagnosis. J Neurooncol. 2017;135(2):381–90.

Publisher's note